An Effective Switching-Table-Based DTC of Five-Phase PMSM for Reduction of Torque Ripples

Rajanikanth Puli, *Student Member, IEEE,* and Vinay Kumar Thippiripati, *Senior Member, IEEE*

***Abstract*— Higher torque and flux ripples exist in conventional direct torque control (DTC) of five-phase permanent magnet synchronous motor (5-ϕ PMSM) drive due to application of single voltage vector over entire control period. Duty-cycle based DTC techniques are proposed for 5-ϕ PMSM recently to achieve superior steady-state responses. However, most of the duty cycle-based schemes are complex. To suppress the ripples in flux and torque, an effective switching table-operated DTC is proposed in which selection of active voltage vector (AVV) for decoupled torque and flux control is introduced for 5-ϕ PMSM. Secondly, the selected AVVs for torque and flux control are applied along with a null vector in two consecutive samples, respectively based on effective duty control scheme. The duty cycles of selected AVVs are determined to meet the reference flux and torques in respective control intervals, which ensures reduced flux and torque ripples. When voltage vector for torque control is applied, the effect on flux is negligible and vice versa, which achieves a decoupled flux and torque control. The proposed DTC is verified experimentally and compared with conventional DTC, conventional model predictive current control (MPCC) scheme, and a duty-cycle control based MPCC for 5-ϕ PMSM. The proposed DTC achieves significant reduction in torque and flux ripples while maintaining comparable dynamic response and computational burden.**

Link to graphical and video abstracts, and to code: https://latamt.ieeer9.org/index.php/transactions/article/view/10348

***Index Terms*— Control period, duty cycle, five-phase permanent magnet synchronous motor, flux ripple, torque ripple.**

I. INTRODUCTION

OWING to the benefits such as better torque density, degree of freedom, fault-tolerance, and power splitting, multi-phase PMSM drive is gaining attention over standard 3-phase PMSM drives. Due to better reliability multiphase drives are becoming superior choice for electric vehicles, and all-electric aircrafts [1]. Modern speed control methods such as DTC and model predictive control (MPC) are widely researched for 5-ϕ PMSM [2]. Noguchi and Takahashi presented DTC of 3-ϕ induction motor in the 1980s for the first time [3]. Later concept of DTC was applied to synchronous machines as well. DTC works on the principle of voltage vector selection using commands of flux and torque hysteresis, and sector of stator flux vector. DTC possess many advantages over FOC such as decoupled flux and torque control, and fast dynamic response [4]. However, DTC has disadvantages too. Higher ripples in flux and torque, inconsistencies in switching frequency are major disadvantages. For reduction of torque ripple, method of shortening of hysteresis band is presented in [5].

However, there was increase in switching frequency and further reduction is not possible due to delay in control algorithm implementation. Later method of duty modulation is presented in [6], in which an AVV followed by a zero-voltage vector (ZVV) is applied. However, it is very crucial to determine the interval for which AVV and ZVV are applied.

A 2-level Voltage Source Inverter (VSI) fed 5-ϕ PMSM has two complex planes called fundamental plane (d_1-q_1) and harmonic plane (d_3-q_3). Due to the existence of d_3-q_3 plane, harmonic currents of low frequency are present, which makes control more complex and it is essential to make the voltages in this plane zero to achieve effective control [7]. In case of 5-ϕ PMSM it is also important to consider the effect of these vectors on the harmonic subspace. So, in 5-ϕ PMSM drives, it becomes more difficult to select suitable voltage vectors which can effectively reduce the torque ripples along with harmonic subspace control. The DTC scheme for 5-ϕ PMSM is introduced first time in [8] with sensor less operation. Although it could provide the control, the stator current profile was not sinusoidal due to incomplete control of d_3-q_3 plane flux. In [9], this scheme is remodified to achieve the flux and current control in d_3-q_3 plane. Subsequently, the flux in d_3-q_3 plane is minimized and current profile was improved. However, ripples in torque and flux are very high. An MPCC based approach with 31 and 21 candidate vectors is presented in [10] for 5-ϕ induction motor. Later in the literature these schemes are considered as MPCC-31 and MPCC-21, respectively. To minimize ripples in flux and torque, a virtual vector (VV) based DTC was presented in [11], [12] to minimize the harmonic currents in d_3-q_3 plane. Another VV based DTC for dual 3-ϕ PMSM was presented in [13] to minimize the harmonic currents and torque ripples. However, these schemes offer complexity in control aspect. Another aspect of 5-ϕ drives is at low speeds, demagnetization can occur. To avoid demagnetization effect, DTC methods for 2-level and 3-level NPC inverter fed 5-ϕ induction motors were presented in [14]-[18]. In [19] and [20] new VV based approaches for reduction of torque ripple are reported for six-phase induction motor. A duty-cycle based MPCC for PMSM was presented in [21] which applies dual vectors in a sample period to obtain the control. The DTC implementation for open-end winding 5-ϕ induction motor were explored in [22] and [23] to eliminate d_3-q_3 plane harmonics. Fault-tolerance capability of 5-ϕ drives were tested in [24]-[27] using concept of VVs. Although various duty-cycle-based and virtual-vector-based DTC schemes have been

The associate editor coordinating the review of this manuscript and approving it for publication was José Miguel Sosa (*Corresponding author: Rajanikanth Puli*).

This work was supported in part by the Anusandhan National Research Foundation (ANRF), under Grant ANRF/IRG/2024/000484/ENS and in part by the National Institute of Technology, Warangal, India. (Corresponding author: Vinay Kumar Thippiripati).

Rajanikanth Puli, and V. K. Thippiripati are with the National Institute of Technology, Warangal, India (e-mails: pr712044@student.nitw.ac.in, and vinaykumar@nitw.ac.in).

reported for ripple reduction in five-phase drives, the use of basic (non-virtual) voltage vectors within a simple lookup-table DTC framework with dedicated torque and flux vectors applied in consecutive sampling periods has not been explored for 5-ϕ PMSM. The proposed method achieves effective decoupling and ripple reduction with lower implementation complexity compared to virtual-vector or multi-vector predictive approaches. Hence, an effective look-up table-based DTC for 5-ϕ PMSM is proposed in this article which uses basic voltage vectors of the complex plane to effectively reduce the ripples in flux and torque.

This paper proposes an effective switching table for AVV selection. In this method, AVV for control of flux and the AVV for control of torque are selected based on flux, torque errors, and stator flux sector information in complex plane. The AVV for torque control along with zero vector and the AVV for flux control along with zero vector are applied in two different and consecutive samples. It is found that this way of application of AVVs in two different samples can help in meeting the reference values of torque and flux thereby reduction in flux and torque ripples. AVVs and null voltage vector are applied so as to obtain only single transition in each control period. Proposed DTC is compared experimentally with conventional DTC, conventional MPCC with 31 voltage vectors (MPCC-31), duty-cycle based control adopted from [21] for 5-ϕ PMSM represented as Duty-based Model Predictive Current Control (DBMPCC).

The major contributions of proposed DTC are given below:

1) An effective switching table to control torque and flux in two consecutive samples is proposed.
2) The effect on flux when torque controlling voltage vector applied is minimal and vice versa, there by achieving the decoupled control.
3) A new duty-cycle approach is presented to meet the reference values of flux and torque effectively. This results in significant reduction of flux and torque ripple.

The rest of this paper is organized as follows. Section-II presents model of 5-ϕ PMSM in stationary frame. Section-III illustrates conventional DTC briefly. Section-IV explains proposed DTC. Experimental results of proposed DTC and its comparison with conventional DTC, MPCC-31, and DBMPCC are shown in section-V. Finally, section-VI concludes this article.

II. Model of Two-level VSI Fed Five-Phase PMSM

A two-level VSI topology was chosen for the five-phase system owing to its structural simplicity, lower cost, and reduced control complexity. With only ten switches, it allows direct application of the classical DTC switching table for fast torque and flux control without requiring a complex modulator. This section presents the dynamic model of 2-level VSI fed 5-ϕ PMSM. Fig. 1 shows the connection diagram of 5-ϕ PMSM operated using a 2-level VSI. The 5-ϕ, 2-level VSI has 32 switching states as shown in Fig. 2 among which 30 are AVV switching states and 2 are null vector switching states. Fig. 2(a) and Fig. 2(b) represents switching states in α_1-β_1 and α_3-β_3 subspaces, respectively.

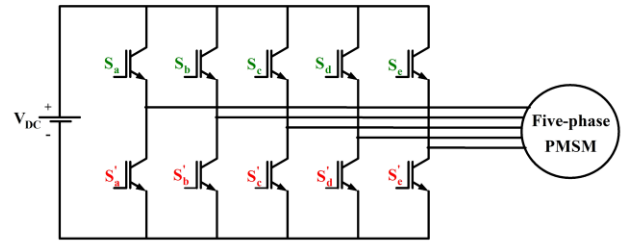

Fig. 1. Five phase 2-level VSI operated 5-ϕ PMSM drive.

In stationary frame of reference, stator voltage and flux linkage equations are represented by (1) and (2) respectively.

$$V_s = R_s I_s + \frac{d\lambda_s}{dt} \quad (1)$$

$$\lambda_s = L_s I_s + (\lambda_r * e^{j\theta_r}) \quad (2)$$

where λ_s, I_s, and V_s are the stator flux linkage, current, and voltage space vectors, respectively.
L_s, R_s are synchronous inductance and per phase stator resistance, respectively. λ_r and θ_r are rotor flux linkage and the rotor position. The torque produced in 5-ϕ PMSM is given by:

$$T_{em} = \frac{5}{2} \cdot \frac{P}{2} \left(\lambda_{\alpha s} i_{\beta s} - \lambda_{\beta s} i_{\alpha s} \right) \quad (3)$$

The relationship between the produced torque and speed is

$$T_{em} = J \frac{d\omega_m}{dt} + B\omega_m + T_{mL} \quad (4)$$

where T_{em} is the developed motor torque, and T_{mL} is the applied load torque. B represents friction coefficient, and ω_m is speed of the rotor in mechanical rad/s.

III. Conventional DTC

The block diagram of conventional DTC [9] is represented by Fig. 3. In conventional DTC, complex plane is partitioned into ten equal sectors each having a span of 36 degrees. Based on the error commands provided from 3-level and 2-level hysteresis controllers for torque and flux, respectively and the stator flux sector, a look-up is designed as presented in Table I. Conventional DTC look-up table provides suitable voltage vector to meet required reference flux, torque so that the speed of the motor is controlled effectively.

IV. Proposed DTC

Conventional DTC technique applies a voltage vector in every sample time to change both stator flux and torque. However, it can't control the magnitudes of flux and torque effectively. In duty-based DTC, every sample contains two vectors (an AVV and a ZVV), which are used to control the torque magnitude. However, it is not possible for stator flux magnitude control using duty-based DTC methods. In order to control the magnitudes of flux and torque effectively a new duty-controlled DTC is proposed.

Proposed DTC method applies two voltage vectors along with null vectors in consecutive sample intervals to control flux and torque in respectively.

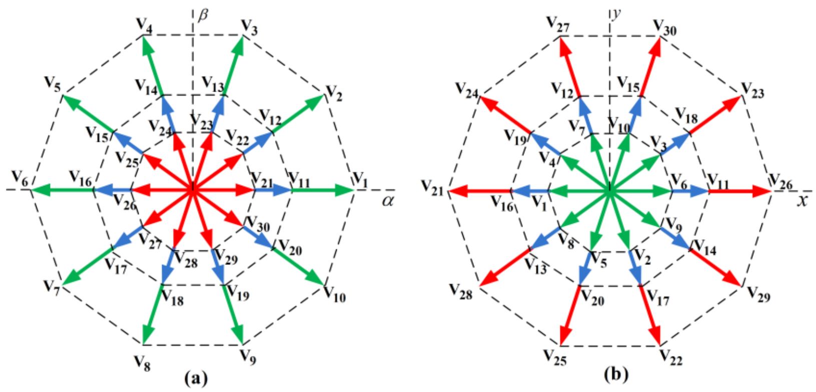

Fig. 2. Five-phase 2-level VSI vector diagram. (a) α_1-β_1 plane. (b) α_3-β_3 plane.

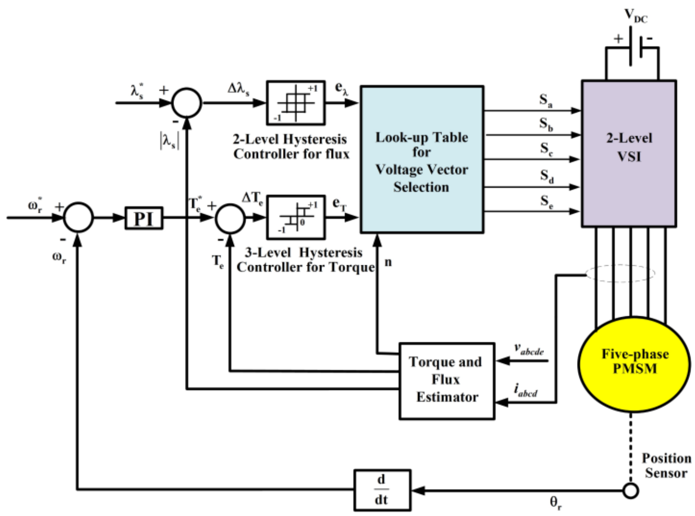

Fig. 3. Control structure of the conventional DTC for 5-ϕ PMSM drive.

TABLE I
CONVENTIONAL DTC LOOK-UP TABLE

		Sector									
e_λ	e_T	1	2	3	4	5	6	7	8	9	10
1	1	V_3	V_4	V_5	V_6	V_7	V_8	V_9	V_{10}	V_1	V_2
	-1	V_4	V_5	V_6	V_7	V_8	V_9	V_{10}	V_1	V_2	V_3
-1	1	V_9	V_{10}	V_1	V_2	V_3	V_4	V_5	V_6	V_7	V_8
	-1	V_8	V_9	V_{10}	V_1	V_2	V_3	V_4	V_5	V_6	V_7

As the voltage vectors are applied in separate sampling intervals, the magnitudes of torque and flux are controlled effectively. The voltage vectors are chosen such that they can bring the required changes in torque and flux separately. Two AVVs which can develop immediate change in flux and torque are chosen and applied in each alternate sample. The voltage vector for torque control (VVTC) is selected such that it can produce rapid change in torque with almost no flux magnitude change. The voltage vector for flux control (VVFC) is selected such that it can produce rapid change in flux without much affecting torque magnitude. As they are applied along with null vector in every sample the duration for which the VVTC and VVFC are applied is calculated. When VVTC and VVFC are applied as per their calculated duty ratios, the reference flux and torque are attained after every two samples. Therefore, the tracking of reference magnitudes of flux and torque is achieved continuously.

A. VVTC and VVFC Selection

In Fig. 4, control diagram of the proposed DTC scheme is shown. In proposed DTC scheme, a 3-level and 2-level hysteresis controllers for torque and flux, respectively and stator flux vector sector number are used to determine the VVTC (V_T) and VVFC (V_λ). The major change in magnitude of flux is obtained by selecting the nearest voltage vectors lying radial to stator flux vector. Similarly, the major change in magnitude of torque is obtained by selecting the nearest voltage vectors lying tangential to stator flux. Fig. 5 depicts the case when stator flux lying in sector-4. Voltage vectors V_3 and V_8 are chosen as VVFC, where V_3 and V_8 effects in immediate increasing and decreasing of stator flux value, respectively. While stator flux value is affected, there is an insignificant change in torque when VVFC is applied.

Similarly, the voltage vectors V_5 and V_{10} are chosen as VVTC, where V_5 produces the change in torque in forward direction and V_{10} produces the change in torque in reverse direction. Similarly, when stator flux lies in sector-1, voltage vectors V_1 and V_6 are chosen as VVFC, where V_1 and V_6 effects in immediate increasing and decreasing of stator flux value, respectively. While stator flux value is affected, there is an insignificant change in torque when VVFC is applied.

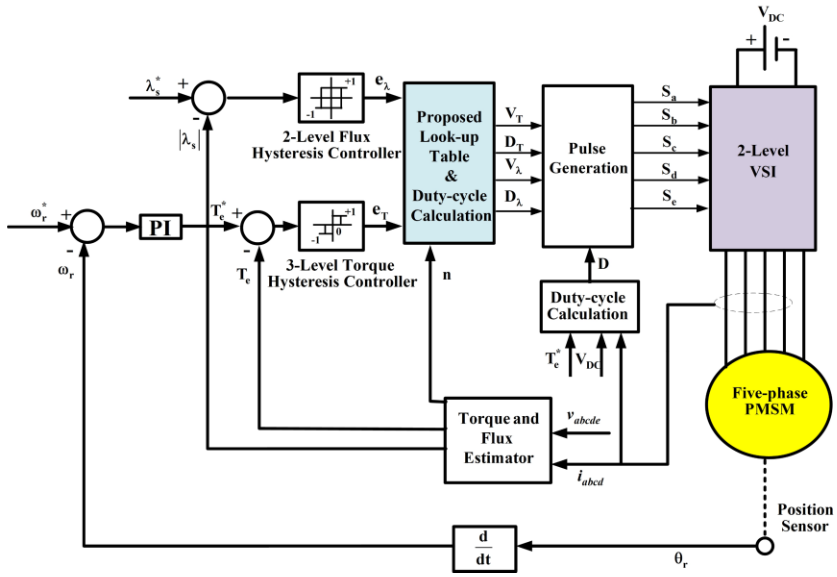

Fig. 4. Proposed DTC block diagram for 5-ϕ PMSM drive.

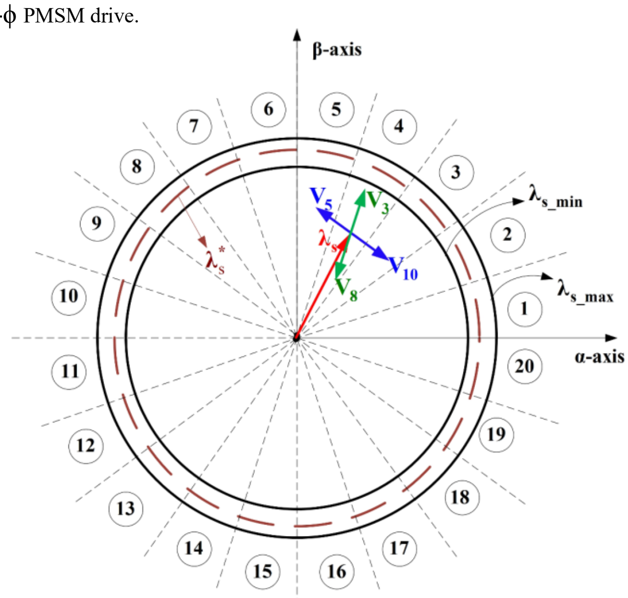

Fig. 5. VVTC and VVFC when stator flux vector is in sector-4 for 5-ϕ PMSM drive.

The voltage vectors V_4 and V_9 are chosen as VVTC, where V_4 increases the torque and V_9 decreases the torque. Application of these voltage vectors can bring immediate change in torque with negligible change in flux. The voltage vector selection criteria for VVTC and VVFC under different sector number, flux hysteresis output (e_λ), and torque hysteresis output (e_T) is shown in Table II.

B. Duty Cycle Calculation

VVTC and VVFC are found for alternate control periods. Selected VVTC and one zero vector applied over initial control period, similarly selected VVFC along with one zero vector is used over the next control period. Duty cycle values of VVTC and VVFC are found to meet the reference torque and flux. To meet stator flux reference, the magnitude of stator flux is changed by applying V_T and V_λ with duty cycles of D_T and D_λ, respectively. Equations (5) and (6) gives stator flux change in the direction of λ_s due to application of V_T and V_λ, respectively.

$$\left|\Delta\lambda_s^{V_T}\right| = D_T\left|V_T\right|T_s\cos(\theta_T - \theta_p) \tag{5}$$

$$\left|\Delta\lambda_s^{V_\lambda}\right| = D_\lambda\left|V_\lambda\right|T_s\cos(\theta_\lambda - \theta_p) \tag{6}$$

where θ_T and θ_λ indicates angles of V_T and V_λ with α-axis. θ_p is the present stator flux angle. The magnitude of overall stator flux after two control periods is given by

$$\left|\lambda_s^*\right| = \left|\lambda_s\right| + \left|\Delta\lambda_s^{V_T}\right| + \left|\Delta\lambda_s^{V_\lambda}\right| \tag{7}$$

When the negligible change in rotor position over a control period is ignored, the discretized stator flux change can be determined from (2) as

TABLE II
PROPOSED VOLTAGE VECTOR LOOKUP-TABLE FOR FIVE-PHASE PMSM FROM SECTOR **1** TO **20**

Sector		**1**		**2**		**3**		**4**		**5**		**6**		**7**		**8**		**9**		**10**	
e_λ	e_T	V_T	V_λ	V_T	V_λ	V_T	V_λ	V_T	V_λ	V_T	V_λ	V_T	V_λ	V_T	V_λ	V_T	V_λ	V_T	V_λ	V_T	V_λ
	1	V_4	V_1	V_4	V_2	V_5	V_2	V_5	V_3	V_6	V_3	V_6	V_4	V_7	V_4	V_7	V_5	V_8	V_5	V_8	V_6
1	**0**	V_{31}	V_{31}	V_0	V_0	V_{31}	V_{31}	V_0	V_0	V_{31}	V_{31}	V_0	V_0	V_{31}	V_{31}	V_0	V_0	V_{31}	V_{31}	V_0	V_0
	-1	V_9	V_1	V_9	V_2	V_{10}	V_2	V_{10}	V_3	V_1	V_3	V_1	V_4	V_2	V_4	V_2	V_5	V_3	V_5	V_3	V_6
	1	V_4	V_6	V_4	V_7	V_5	V_7	V_5	V_8	V_6	V_8	V_6	V_9	V_7	V_9	V_7	V_{10}	V_8	V_{10}	V_8	V_1
-1	**0**	V_0	V_0	V_{31}	V_{31}	V_0	V_0	V_{31}	V_{31}	V_0	V_0	V_{31}	V_{31}	V_0	V_0	V_{31}	V_{31}	V_0	V_0	V_{31}	V_{31}
	-1	V_9	V_6	V_9	V_7	V_{10}	V_7	V_{10}	V_8	V_1	V_8	V_1	V_9	V_2	V_9	V_2	V_{10}	V_3	V_{10}	V_3	V_1
Sector		**11**		**12**		**13**		**14**		**15**		**16**		**17**		**18**		**19**		**20**	
e_λ	e_T	V_T	V_λ	V_T	V_λ	V_T	V_λ	V_T	V_λ	V_T	V_λ	V_T	V_λ	V_T	V_λ	V_T	V_λ	V_T	V_λ	V_T	V_λ
	1	V_9	V_6	V_9	V_7	V_{10}	V_7	V_{10}	V_8	V_1	V_8	V_1	V_9	V_2	V_9	V_2	V_{10}	V_3	V_{10}	V_3	V_1
1	**0**	V_{31}	V_{31}	V_0	V_0	V_{31}	V_{31}	V_0	V_0	V_{31}	V_{31}	V_0	V_0	V_{31}	V_{31}	V_0	V_0	V_{31}	V_{31}	V_0	V_0
	-1	V_4	V_6	V_4	V_7	V_5	V_7	V_5	V_8	V_6	V_8	V_6	V_9	V_7	V_9	V_7	V_{10}	V_8	V_{10}	V_8	V_1
	1	V_9	V_1	V_9	V_2	V_{10}	V_2	V_{10}	V_3	V_1	V_3	V_1	V_4	V_2	V_4	V_2	V_5	V_3	V_5	V_3	V_6
-1	**0**	V_0	V_0	V_{31}	V_{31}	V_0	V_0	V_{31}	V_{31}	V_0	V_0	V_{31}	V_{31}	V_0	V_0	V_{31}	V_{31}	V_0	V_0	V_{31}	V_{31}
	-1	V_4	V_1	V_4	V_2	V_5	V_2	V_5	V_3	V_6	V_3	V_6	V_4	V_7	V_4	V_7	V_5	V_8	V_5	V_8	V_6

$$\Delta\lambda_s = L_s \Delta I_s \tag{8}$$

$$\Delta\lambda_s^{\perp} = L_s \Delta I_s^{\perp} \tag{9}$$

where $\Delta I_s^{\perp}$ is perpendicular component of ΔI_s. If q-axis component of λ_s is assumed as $I_s^{\perp}$, then $\Delta I_s^{\perp}$ can be found using

$$\Delta I_s^{\perp} = I_{qs}^{*} - I_s^{\perp} \tag{10}$$

where I_{qs}^{*} is stator q-axis current reference. In surface mounted 5-ϕ PMSM, relation between reference torque and reference q-axis currents is given by:

$$T_{em}^{*} = \left(\frac{5}{2}\right)\left(\frac{P}{2}\right)\lambda_r I_{qs}^{*} \tag{11}$$

The VVTC is responsible to obtain the change in torque in order to meet the reference torque and it can be achieved by the application of V_T and V_λ at their respective duty cycles. The overall change in magnitude of stator flux in the perpendicular direction of λ_s when V_T and V_λ are applied in consecutive control periods can be found as

$$\Delta\lambda_s^{\perp} = D_T \left|V_T\right| T_s \sin(\theta_T - \theta_p) + D_\lambda \left|V_\lambda\right| T_s \sin(\theta_\lambda - \theta_p) \tag{12}$$

By solving the equations (5)-(12), duty cycles for V_T and V_λ can be obtained as

$$D_\lambda = \frac{\delta\lambda_{V_T}^{\perp}\,\delta\lambda - \delta\lambda_{V_T}\,\delta\lambda^{\perp}}{\delta\lambda_{V_\lambda}\,\delta\lambda_{V_T}^{\perp} - \delta\lambda_{V_\lambda}^{\perp}\,\delta\lambda_{V_T}} \tag{13}$$

$$D_T = \frac{\delta\lambda_{V_\lambda}\,\delta\lambda^{\perp} - \delta\lambda_{V_\lambda}^{\perp}\,\delta\lambda}{\delta\lambda_{V_\lambda}\,\delta\lambda_{V_T}^{\perp} - \delta\lambda_{V_\lambda}^{\perp}\,\delta\lambda_{V_T}} \tag{14}$$

where $\delta\lambda_{V_T}$ is the change in stator flux magnitude in the direction of V_T and expressed as $\delta\lambda_{V_T} = \left|V_T\right| T_s \cos(\theta_T - \theta_p)$;

$\delta\lambda_{V_\lambda}$ is the change in stator flux magnitude in the direction of V_λ and expressed as $\delta\lambda_{V_\lambda} = \left|V_\lambda\right| T_s \cos(\theta_\lambda - \theta_p)$;

$\delta\lambda$ is error between stator reference flux magnitude and stator actual flux magnitude $\delta\lambda = \left|\lambda_s^{*}\right| - \left|\lambda_s\right|$;

$\delta\lambda^{\perp}$ is component of stator flux vector change perpendicular to λ_s, $\delta\lambda^{\perp} = L_s\left[\frac{T_{ref}}{(5P/4)\lambda_r} - \left|I_s\right| \sin(\theta_i - \theta_p)\right]$.

where θ_i is the angle subtended by stator current. Phasor diagram of the proposed DTC scheme is illustrated in Fig. 6.

In this figure the effect of VVTC and VVFC on stator flux is indicated. Where $D_\lambda V_\lambda T_s$ is the change in magnitude of flux under application of VVFC. Similarly, the torque requirement can be achieved by changing the flux by $D_T V_T T_s$ by the application of VVTC. The effect of VVTC and VVFC on the stator flux and torque trajectories is presented in Fig. 7 when torque and flux errors are 1, -1, respectively when stator flux is complex plane's sector-2.

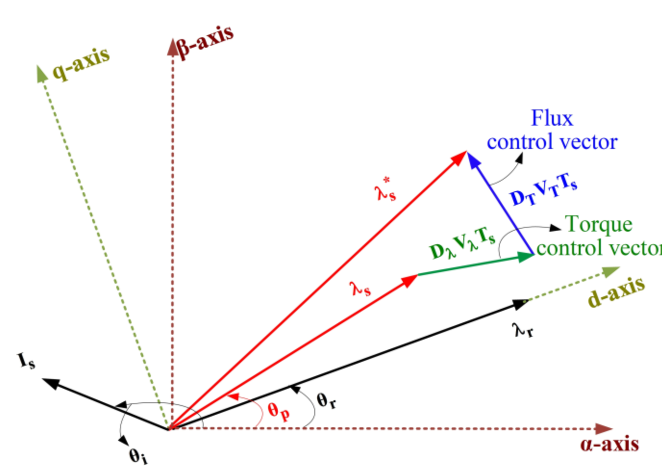

Fig. 6. Proposed DTC phasor diagram scheme for 5-ϕ PMSM drive.

Fig. 7 shows that when VVTC is applied effect on flux is negligible and when VVFC is applied impact on the torque is minimal. Hence, a decoupled flux and torque control can be achieved after every two consecutive control periods. The control flow of proposed DTC scheme is presented in Fig. 8.

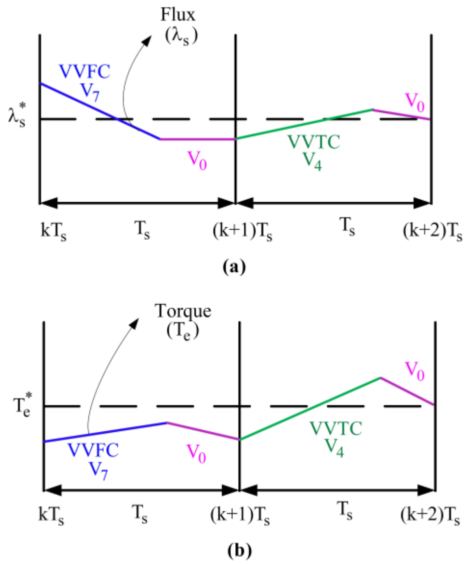

Fig. 7. Effect of VVFC and VVTC on (a) Flux (b) Torque.

When VVTC is applied, the angle between the selected voltage vector and the stator flux vector is close to 90° (tangential), resulting in a very small radial component. Therefore, the change in flux magnitude is theoretically negligible:

$$\Delta|\lambda_s|^{V_T} = D_T|V_T|T_s\cos(\theta_T-\theta_p)\approx 0 \qquad (15)$$

Since $\theta_T - \theta_p \approx \pm 90$ degree. Similarly, for VVFC (radial), the tangential component responsible for torque variation is minimal.

C. *Harmonic Subspace (α_3-β_3) Consideration*

Although the proposed DTC is developed in the fundamental (α_1-β_1) plane, it implicitly limits the voltage components in the harmonic (α_3-β_3) subspace. In a five-phase two-level VSI, each voltage vector produces components in both α_1-β_1 and α_3-β_3 planes. Large vectors in the fundamental plane generally correspond to small vectors in the harmonic plane. In the proposed method, the selected VVFC (radial to stator flux) and VVTC (tangential to stator flux) are applied only for short durations $D_\lambda T_s$ and $D_T T_s$ (where D_T, D_λ<1) along with zero vectors in two consecutive sampling periods. The net third harmonic flux change over two sampling periods is given by:

$$\Delta\lambda_{s3} = D_T T_s \cdot V_{T3} + D_\lambda T_s \cdot V_{\lambda 3} \qquad (15)$$

where V_{T3} and $V_{\lambda 3}$ are the projections of VVTC and VVFC in the α_3-β_3 plane. These vectors have non-collinear and relatively small projections in the α_3-β_3 plane.

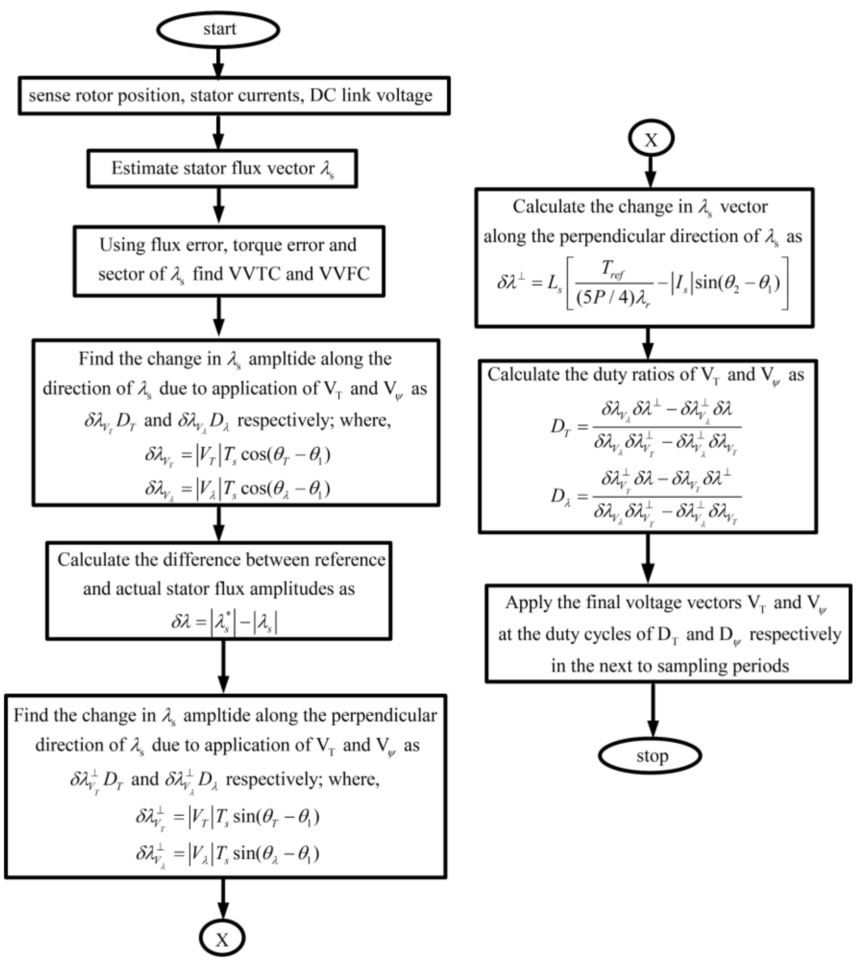

Fig. 8. Proposed DTC flowchart for 5-ϕ PMSM drive.

Combined with short duty cycles and alternation with zero vectors, their contributions partially cancel, keeping the net volt-second integral (and thus $\Delta\lambda_{s3}$) small. This inherently restricts low-order harmonic currents without using virtual vectors or dedicated harmonic controllers.

V. Experimental Results

A. Description of Hardware

The proposed scheme's effectiveness is verified by comparing the experiments results with conventional DTC and MPCC-31 schemes. To implement the proposed control algorithm, dSPACE-1104 controller along with MATLAB/Simulink environment is used. A 5-ϕ PMSM along with a coupled DC generator is used where DC generator and resistive load acts as load. An incremental encoder (1024 pulse) is used for sensing the position and speed of the motor. One voltage sensor, four hall-effect current sensors, are used to sense DC link voltage, phase currents, respectively. The set up used for experimental implementation is presented in Fig. 9. Parameters of 5-ϕ PMSM are tabulated in Table III.

TABLE III
Parameters of Five-Phase PMSM

Parameter	Value
Rated voltage	300 V
Rated Current	3.4 A
Rated Power	2.2 kw
Stator resistance	1.45 Ω
Poles	4
Synchronous inductance	0.022 H
Permanent magnet flux	0.5 Wb
Rated speed	1500 RPM

B. Experimental Results

The various control schemes chosen are experimentally tested under both dynamic and steady-state operations. Steady-state operation is tested under no-load as well as loaded-conditions. The dynamic operations are performed by varying the speed and load suddenly. These experimentations on various schemes are performed to evaluate their ripples in flux and torque. Experimental results are found at equal sampling period of 140 µs in all the considered schemes to have a fair comparison. While conducting the comparative experimentations, the limits of flux and torque hysteresis controllers are maintained same for all the methods. Results show that in proposed DTC, the flux and torque ripples under steady-state are reduced effectively compared to conventional DTC, MPCC-31 [10], and DBMPCC schemes. Although MPCC-31V is originally proposed for a five-phase induction motor [10], the 31-vector enumeration and cost function are directly adaptable to PMSM (replacing back-EMF terms). The DBMPCC scheme was implemented by adapting the dual-vector duty-cycle MPCC of [21] (originally for 3-phase) to the five-phase system. The cost function was extended to five-phase currents in the α1-β1 plane while maintaining zero voltage in the α3-β3 plane using the same 31-vector enumeration as MPCC-31. Duty cycles for the two active vectors were calculated analytically following the same principle as [21]. The steady-state responses at 500 rpm, 1250 rpm under no-load are presented in Fig. 10 and Fig.11, respectively. The steady-state responses are obtained under the application of 50% load at various speeds such as 500 rpm, 750 rpm. The current, flux, torque and speed results are obtained and presented in Fig. 12 when motor was running at a speed of 500 rpm and 50 % of rated load. Similarly, these responses are obtained and presented in Fig. 13 when motor was running at 750 rpm and 50% of rated load.

Fig. 9. Experimental test bench for 5-ϕ PMSM drive.

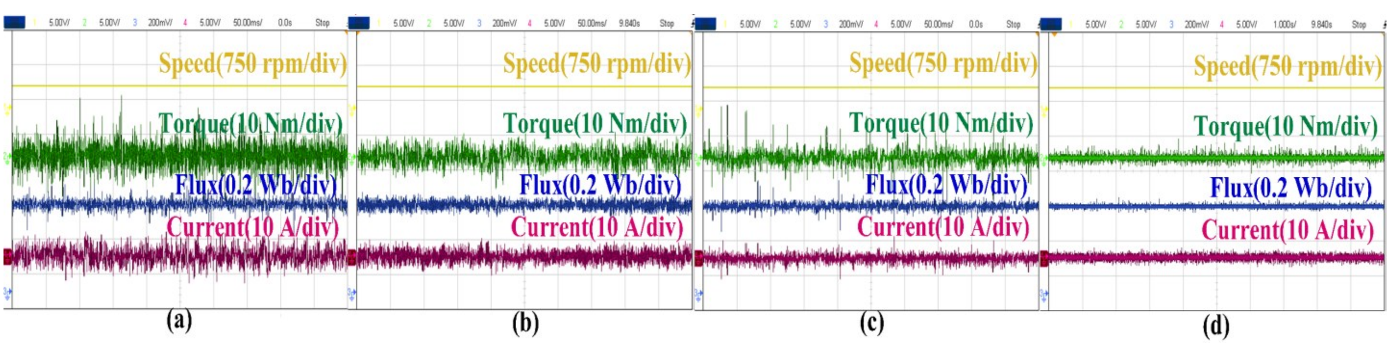

Fig. 10. Responses under steady-state at 500 rpm, no-load. (a) Conventional DTC [9]. (b) MPCC-31 [10]. (c) DBMPCC [21]. (d) Proposed DTC.

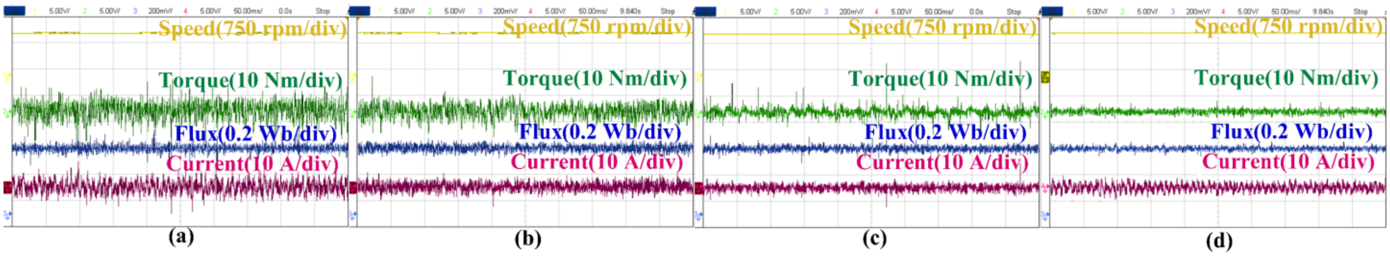

Fig. 11. Responses under steady-state at 1250 rpm, no-load. (a) Conventional DTC [9]. (b) MPCC-31 [10]. (c) DBMPCC [21]. (d) Proposed DTC.

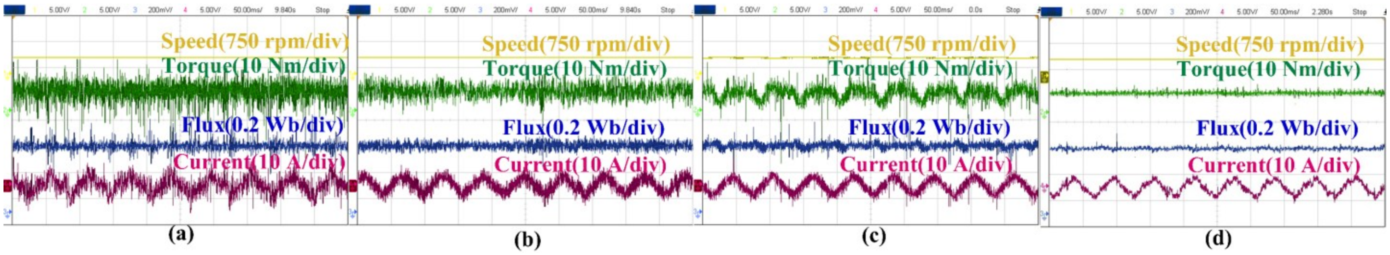

Fig. 12. Responses under steady-state at 500 rpm, 50% load. (a) Conventional DTC [9]. (b) MPCC-31 [10]. (c) DBMPCC [21]. (d) Proposed DTC.

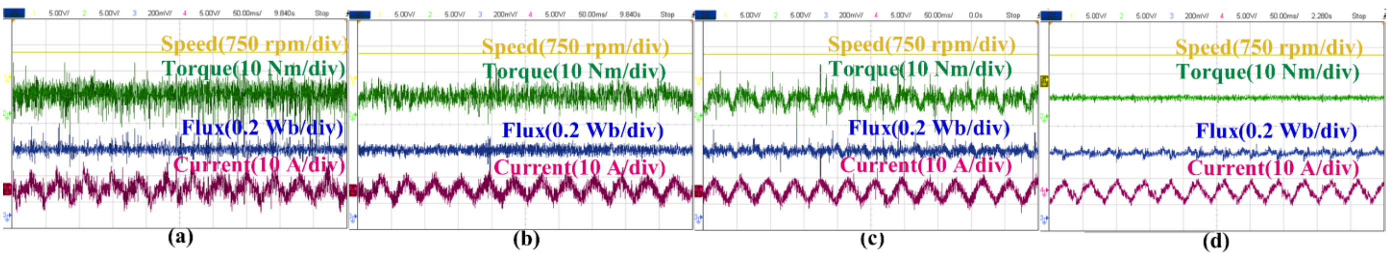

Fig. 13. Responses under steady-state at 750 rpm, 50% load. (a) Conventional DTC [9]. (b) MPCC-31 [10]. (c) DBMPCC [21]. (d) Proposed DTC.

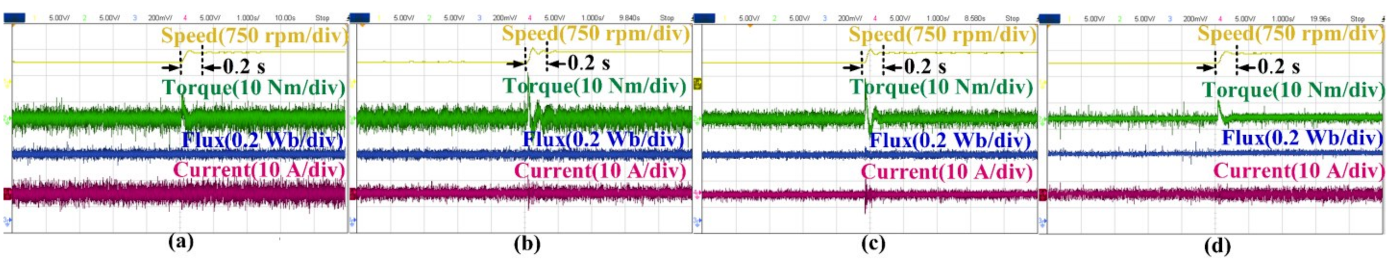

Fig. 14. Dynamic responses for step speed change from 600 rpm to 900 rpm at no-load. (a) Conventional DTC [9]. (b) MPCC-31 [10]. (c) DBMPCC [21]. (d) Proposed DTC.

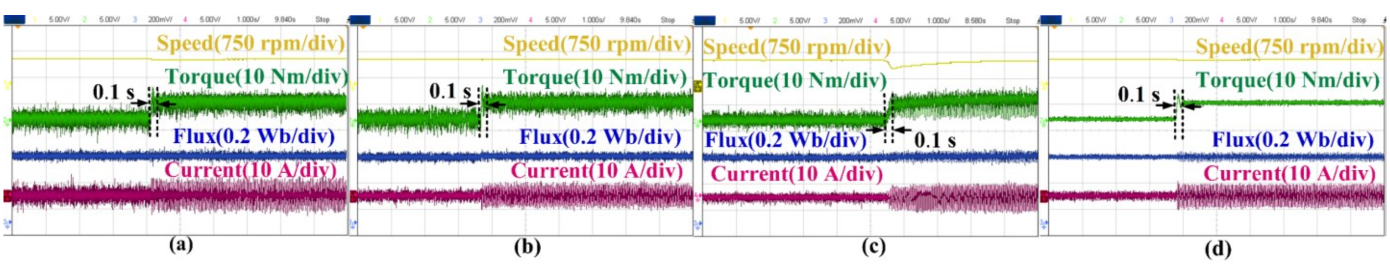

Fig. 15. Dynamic responses at a speed of 750 rpm when load applied suddenly. (a) Conventional DTC [9]. (b) MPCC-31 [10]. (c) DBMPCC [21]. (d) Proposed DTC.

Standard deviation concept is employed to calculate flux and torque ripples. Equations used for calculating the ripples in flux and torque are given by:

$$T_{e\_ripple} = \sqrt{\frac{1}{N}\sum_{j=0}^{N}(T_e(j) - T_e^*)^2} \tag{15}$$

$$\psi_{ripple} = \sqrt{\frac{1}{N}\sum_{j=0}^{N}(\psi_s(j) - \psi_s^*)^2} \tag{16}$$

Dynamic responses are obtained for sudden variation in load and speed for all the considered schemes. Fig. 14 shows the responses of current, torque, flux, and speed when motor speed changes from 600 rpm to 900 rpm under no-load condition. These responses shows that proposed scheme is offering a similar dynamic response as that of conventional DTC, MPCC-31, and DBMPCC. However, the steady-state results in proposed scheme found to be much better when compared with conventional DTC, MPCC-31, and DBMPCC schemes. The dynamic responses when load is suddenly changed from no-load to 50% of the full-load is presented in Fig. 15 for considered three schemes. The quantitative comparison of experimental results is presented in Table IV. THD values for stator phase current under different speeds and load conditions are now reported for all compared methods. The THD spectra for various considered schemes are presented in the revised manuscript as shown in Fig. 18 and Fig. 19.

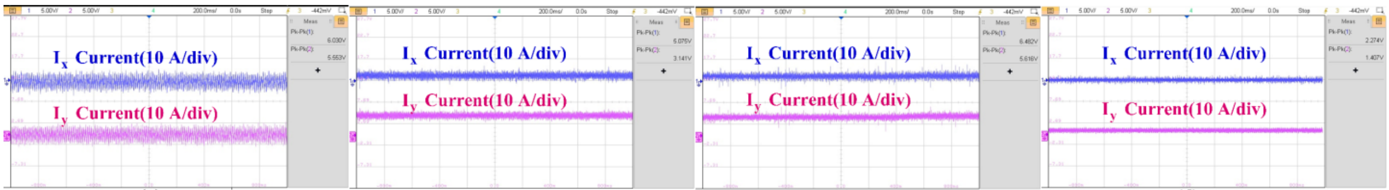

(a) (b) (c) (d)

Fig. 16. Responses of i_x and i_y harmonic currents at 750 rpm, no-load. (a) Conventional DTC [9]. (b) MPCC-31 [10]. (c) DBMPCC [21]. (d) Proposed DTC.

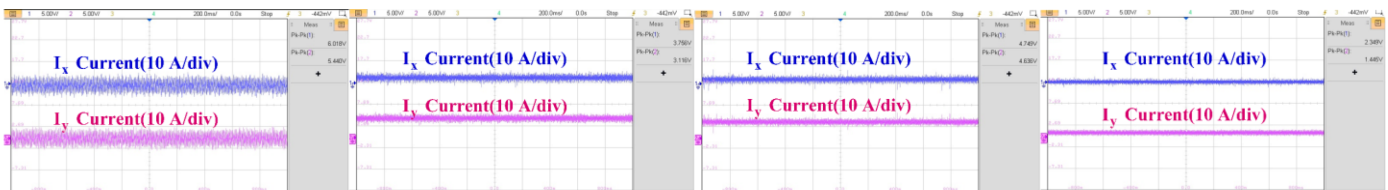

(a) (b) (c) (d)

Fig. 17. Responses of i_x and i_y harmonic currents at 1000 rpm, no-load. (a) Conventional DTC [9]. (b) MPCC-31 [10]. (c) DBMPCC [21]. (d) Proposed DTC.

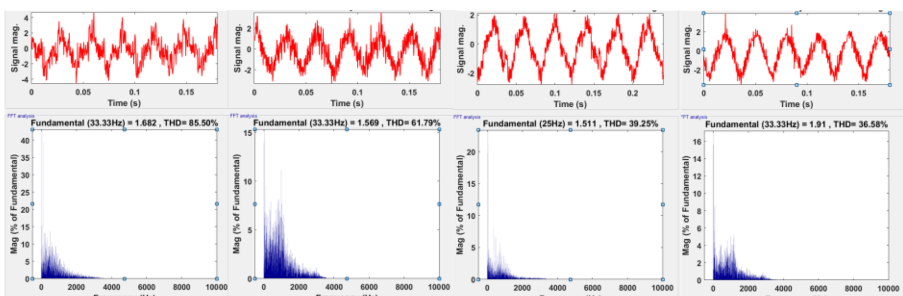

(a) (b) (c) (d)

Fig. 18. THD spectra for different considered schemes at 1000 rpm, 50% load. (a) Conventional DTC [9]. (b) MPCC-31 [10]. (c) DBMPCC [21]. (d) Proposed DTC.

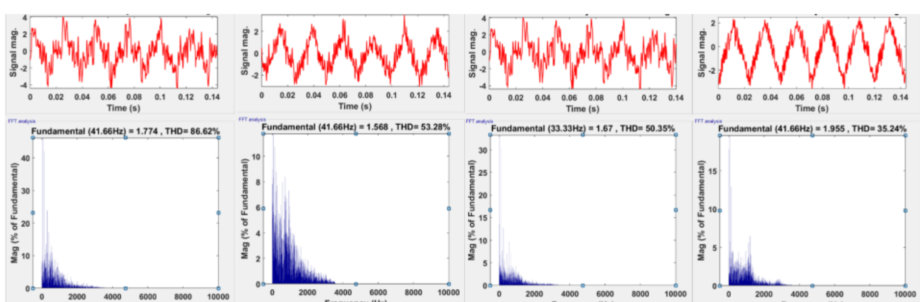

(a) (b) (c) (d)

Fig. 19. THD spectra for different considered schemes at 1250 rpm, 50% load. (a) Conventional DTC [9]. (b) MPCC-31 [10]. (c) DBMPCC [21]. (d) Proposed DTC.

Experimental results from Table IV show that there is a significant flux and torque ripple reduction, in the case of proposed DTC, compared to MPCC-31, conventional DTC, and DBMPCC schemes. The switching frequencies of conventional DTC, MPCC-31, DBMPCC, and proposed DTC schemes are found to be 1815 Hz, 1773 Hz, 2396 Hz, and 2306 Hz, respectively. Although the average switching frequency of the proposed DTC (2306 Hz) is higher than conventional DTC

(1815 Hz) and MPCC-31 (1773 Hz), it remains lower than DBMPCC (2396 Hz). The experimentally calculated switching losses increased by only approximately 10–15% compared to conventional DTC which are calculated using device datasheet parameters and measured current. This modest increase is largely compensated by the dramatic ripple reduction (torque ripple reduced by 65–75%, flux ripple reduced by 45–60%), which reduces core losses and torque-induced mechanical vibrations. Overall efficiency remains comparable or slightly better under loaded conditions due to lower harmonic losses. Table V presents the comparison of execution time for various considered scheme and proposed DTC. The computation time is effectively reduced in the proposed DTC when compared with MPCC31 and DMPCC schemes.

TABLE IV
SWITCHING FREQUENCY, FLUX RIPPLE, TORQUE RIPPLE FOR DIFFERENT CONSIDERED SCHEMES

Speed (RPM)	Load Torque (%)	Conventional DTC [9]			MPCC-31 [10]			DBMPCC [21]			Proposed DTC		
		T_{e_ripple} (N.m)	Ψ_{ripple} (m Wb)	f_{sw} (Hz)	T_{e_ripple} (N.m)	Ψ_{ripple} (m Wb)	f_{sw} (Hz)	T_{e_ripple} (N.m)	Ψ_{ripple} (m Wb)	f_{sw} (Hz)	T_{e_ripple} (N.m)	Ψ_{ripple} (m Wb)	f_{sw} (Hz)
500	**0**	1.5104	0.0218	1990	1.1115	0.0218	1621	0.8469	0.0165	2495	0.4504	0.0113	2603
	50	1.7522	0.0301	1956	1.2057	0.0236	2238	1.2670	0.0236	2702	0.3578	0.0110	2712
750	**0**	1.4647	0.0223	1875	1.1553	0.0194	1604	0.8444	0.0163	2613	0.2593	0.0058	2431
	50	1.6448	0.0254	1891	1.2531	0.0231	2092	1.2241	0.0241	2768	0.2389	0.0154	2596
1000	**0**	1.4897	0.0209	1766	1.1899	0.0199	1514	0.7544	0.0169	2334	0.3569	0.0080	2136
	50	1.5616	0.0236	1767	1.2606	0.0213	1928	1.3746	0.0237	2208	0.3255	0.0155	2210
1250	**0**	1.4367	0.0197	1646	1.2584	0.0129	1474	0.6677	0.0157	2057	0.4107	0.0107	1837
	50	1.5900	0.0228	1631	1.3176	0.0227	1716	1.6658	0.0215	1993	0.6593	0.0211	1926

TABLE V
THD AND THIRD HARMONIC CONTENT FOR VARIOUS CONSIDERED SCHEMES

Speed (RPM)	Load Torque (%)	Conventional DTC [9]		MPCC-31 [10]		DBMPCC [21]		Proposed DTC	
		THD (%)	3rd Harmonic	THD (%)	3rd Harmonic	THD (%)	3rd Harmonic	THD (%)	3rd Harmonic
1000	**50**	85.50	39.17	61.79	29.55	39.25	14.5	36.58	12.95
1250	**50**	86.62	41.99	53.28	20.72	50.35	21.2	35.24	8.71

The computational time values of proposed DTC and conventional DTC are almost close. The proposed voltage vector selection offers decoupled flux and torque control in the two successive samples. It is evident from the obtained experimental results that significant reduction of flux and torque ripples is achieved.

TABLE V
COMPUTATIONAL TIME

Control Method	Execution Time
Conventional DTC [9]	99 μs
MPCC31 [10]	128 μs
DBMPCC [21]	130 μs
Proposed DTC	105 μs

Hence, the proposed DTC is effective for the reduction of ripples in torque and flux of 5-ϕ PMSM drive. The proposed DTC shows significantly lower harmonic current amplitudes in the x-y plane than conventional DTC, MPCC-31 and DBMPCC. Quantitative peak values of harmonic currents are provided in Table VI. Fig. 20 presents responses at 100% rated load for two methods conventional DTC and proposed DTC at 1300 rpm.

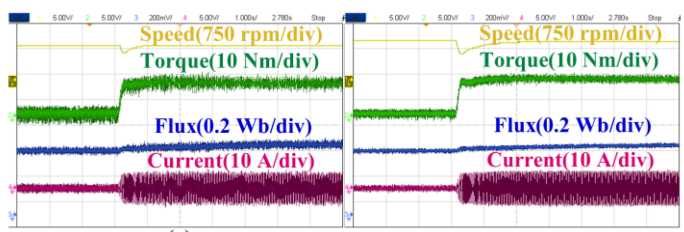

(a) (b)

Fig. 20. Steady-state responses at 1300 rpm and load change from no-load to full-load (a) Conventional DTC (b) Proposed DTC.

TABLE VI
PEAK VALUES OF HARMONIC CURRENTS FOR VARIOUS CONSIDERED SCHEMES

Speed (RPM)	Conventional DTC [9]		MPCC-31 [10]		DBMPCC [21]		Proposed DTC	
	I_x A (peak)	I_y A (peak)	I_x A (peak)	I_y A (peak)	I_x A (peak)	I_y A (peak)	I_x A (peak)	I_y A (peak)
750	3.015	2.77	2.53	1.57	3.24	2.80	1.135	0.7
1000	3.005	2.72	1.875	1.55	2.37	2.31	1.17	0.72

C. Effect of R_S and L_S Variation

The performance of the proposed DTC scheme when subjected to the variation in machine parameters is investigated. For this, the stator resistance and inductance in the control algorithm are increased and decreased by 30%. While executing the proposed DTC method for parameter mismatch, the values of the parameters of Rs and Ls are increased and decreased by 30% from their actual values. The responses of speed, flux, and torque of the five-phase PMSM are obtained before and after the change in PMSM parameters. The responses of flux, speed, and torque of the five-phase PMSM, with and without disturbance of R_s and L_s, are presented in Fig. 21 and Fig. 22, respectively, under steady-state condition.

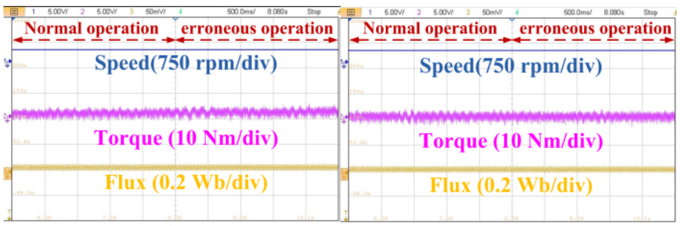

(a) (b)

Fig. 21. Steady-state responses at 400 r/min speed for change in R_s (a) 30% increase. (b) 30% decrease.

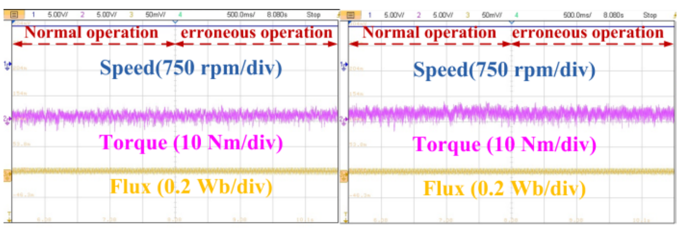

(a) (b)

Fig. 22. Steady-state responses at 1200 r/min speed for change in L_s (a) 30% increase. (b) 30% decrease.

The response with parameter mismatch shows no major changes in steady-state torque and flux. The stator flux linkages in both the situations are almost identical to minor differences in their ripple, irrespective of the variations in PMSM parameters.

VI. Conclusion

This paper presents a new lookup-table-based direct torque control (DTC) strategy for a five-phase permanent magnet synchronous motor (5-ϕ PMSM) drive that effectively reduces both torque and flux ripples while maintaining fast dynamic response. By employing separate voltage vectors for decoupled torque and flux control along with zero voltage vectors in two consecutive sampling periods and calculating appropriate duty cycles, the proposed scheme achieves excellent decoupling between torque and flux. The practical significance of the proposed DTC lies in its ability to deliver significantly lower steady-state ripples compared to conventional DTC, model predictive current control (MPCC), and existing duty-cycle-based methods, without markedly increasing computational complexity. Torque ripple reduced by approximately 65–75% compared to conventional DTC, 55–70% compared to MPCC-31, and 40–55% compared to DBMPCC. Flux ripple reduced by approximately 45–60% compared to conventional DTC, 35–50% compared to MPCC-31, and 25–45% compared to DBMPCC. This makes it particularly attractive for high-performance industrial applications, electric vehicles, and ship propulsion systems where multi-phase drives are preferred for their fault-tolerant capabilities and high-power density. Experimental results confirm that the method maintains dynamic performance comparable to conventional DTC while substantially improving steady-state behavior. However, the primary limitations of the proposed DTC are dependence on accurate motor parameter estimation, and a modest increase in average switching frequency which is acceptable and well-justified trade-off for the achieved performance gains. Future research directions include extending the proposed strategy to sensor less operation, investigating its performance under faulty conditions to exploit the inherent redundancy of five-phase machines, and adapting the control scheme for other multi-phase motor topologies. Additionally, real-time hardware-in-the-loop validation and efficiency analysis under varying operating temperatures will be explored.

References

[1] P. C. Mavila and P. P. Rajeevan, "A Reactive Voltage Compensation-Based Control Scheme to Extend Speed Range in Five Phase Open-End Winding Induction Motor Drives," in IEEE Access, vol. 11, pp. 126843-126856, 2023, doi: 10.1109/ACCESS.2023.3332203.

[2] T. Tao, W. Zhao, Y. He, Y. Cheng, S. Saeed and J. Zhu, "Enhanced Fault-Tolerant Model Predictive Current Control for a Five-Phase PM Motor With Continued Modulation," *IEEE Transactions on Power Electronics*, vol. 36, no. 3, pp. 3236-3246, March 2021, doi: 10.1109/TPEL.2020.3018302.

[3] I. Takahashi and T. Noguchi, "A New Quick-Response and High-Efficiency Control Strategy of an Induction Motor," *IEEE Transactions on Industry Applications*, vol. IA-22, no. 5, pp. 820-827, Sept. 1986, doi: 10.1109/TIA.1986.4504799.

[4] F. Niu, B. Wang, A. S. Babel, K. Li and E. G. Strangas, "Comparative Evaluation of Direct Torque Control Strategies for Permanent Magnet Synchronous Machines," in IEEE Transactions on Power Electronics, vol. 31, no. 2, pp. 1408-1424, Feb. 2016, doi: 10.1109/TPEL.2015.2421321.

[5] J.W. Kang and S.K. Sul, "Analysis and prediction of inverter switching frequency in direct torque control of induction machine based on hysteresis bands and machine parameters," *IEEE Transactions on Industrial Electronics*, vol. 48, no. 3, pp. 545-553, June 2001, doi: 10.1109/41.925581.

[6] Z. Zhang and X. Liu, "A Duty Ratio Control Strategy to Reduce Both Torque and Flux Ripples of DTC for Permanent Magnet Synchronous Machines," *IEEE Access*, vol. 7, pp. 11820-11828, 2019, doi: 10.1109/ACCESS.2019.2892121.

[7] L. Parsa and H. A. Toliyat, "Five-phase permanent-magnet motor drives," *IEEE Transactions on Industry Applications*, vol. 41, no. 1, pp. 30-37, Jan.-Feb. 2005, doi: 10.1109/TIA.2004.841021.

[8] L. Parsa and H. A. Toliyat, "Sensorless Direct Torque Control of Five-Phase Interior Permanent-Magnet Motor Drives," *IEEE Transactions on Industry Applications*, vol. 43, no. 4, pp. 952-959, July-aug. 2007, doi: 10.1109/TIA.2007.900444.

[9] Y. Gao and L. Parsa, "Modified Direct Torque Control of Five-Phase Permanent Magnet Synchronous Motor Drives," *APEC 07 - Twenty-Second Annual IEEE Applied Power Electronics Conference and Exposition*, Anaheim, CA, USA, 2007, pp. 1428-1433, doi: 10.1109/APEX.2007.357704.

[10] C. S. Lim, N. A. Rahim, W. P. Hew, M. Jones and E. Levi, "Model predictive current control of a 5-phase induction motor," *IECON 2011 - 37th Annual Conference of the IEEE Industrial Electronics Society*, Melbourne, VIC, Australia, pp. 1934-1940, 2011, doi: 10.1109/IECON. 2011.6119602.

[11] L. Zheng, J. E. Fletcher, B. W. Williams and X. He, "A Novel Direct Torque Control Scheme for a Sensorless Five-Phase Induction Motor Drive," *IEEE Transactions on Industrial Electronics*, vol. 58, no. 2, pp. 503-513, Feb. 2011, doi: 10.1109/TIE.2010.2047830.

[12] L. Gao, J. E. Fletcher and L. Zheng, "Low-Speed Control Improvements for a Two-Level Five-Phase Inverter-Fed Induction Machine Using Classic Direct Torque Control," *IEEE Transactions on Industrial Electronics*, vol. 58, no. 7, pp. 2744-2754, July 2011, doi: 10.1109/TIE.2010.2070775

[13] Y. Ren and Z. Q. Zhu, "Reduction of Both Harmonic Current and Torque Ripple for Dual Three-Phase Permanent-Magnet Synchronous Machine Using Modified Switching-Table-Based Direct Torque Control," *IEEE Transactions on Industrial Electronics*, vol. 62, no. 11, pp. 6671-6683, Nov. 2015, doi: 10.1109/TIE.2015.2448511.

[14] S. Payami and R. K. Behera, "An Improved DTC Technique for Low-Speed Operation of a Five-Phase Induction Motor," *IEEE Transactions on Industrial Electronics*, vol. 64, no. 5, pp. 3513-3523, May 2017, doi: 10.1109/TIE.2017.2652397.

[15] Y. N. Tatte and M. V. Aware, "Torque Ripple and Harmonic Current Reduction in a Three-Level Inverter-Fed Direct-Torque-Controlled Five-Phase Induction Motor," *IEEE Transactions on Industrial Electronics*, vol. 64, no. 7, pp. 5265-5275, July 2017, doi: 10.1109/TIE.2017.2677346.

[16] S. Payami, R. K. Behera and A. Iqbal, "DTC of Three-Level NPC Inverter Fed Five-Phase Induction Motor Drive With Novel Neutral Point Voltage Balancing Scheme*," IEEE Transactions on Power Electronics*, vol. 33, no. 2, pp. 1487-1500, Feb. 2018 , doi: 10.1109/TPEL.2017.2675621.

[17] Y. N. Tatte, M. V. Aware, J. K. Pandit and R. Nemade, "Performance Improvement of Three-Level Five-Phase Inverter-Fed DTC-Controlled Five-Phase Induction Motor During Low-Speed Operation," *IEEE Transactions on Industry Applications*, vol. 54, no. 3, pp. 2349-2357, May-June 2018, doi: 10.1109/TIA.2018.2798593.

[18] B. Chikondra, A. G. Yepes, O. Al Zaabi, K. Al Hosani, J. Doval Gandoy and R. K. Behera, "Open-Phase Fault-Tolerant DTC Technique for Three-Level NPC VSI-Fed Five-Phase Induction Motor Drives," in IEEE Journal of Emerging and Selected Topics in Power Electronics, vol. 11, no. 2, pp. 2114-2125, April 2023, doi: 10.1109/JESTPE.2022.3224529.

[19] J. K. Pandit, M. V. Aware, R. V. Nemade and E. Levi, "Direct Torque Control Scheme for a Six-Phase Induction Motor With Reduced Torque Ripple," *IEEE Transactions on Power Electronics*, vol. 32, no. 9, pp. 7118-7129, Sept. 2017, doi: 10.1109/TPEL.2016.2624149.

[20] M. H. Holakooie, G. Iwanski and T. Miazga, "Five-Dimensional Switching-Table-Based Direct Torque Control of Six-Phase Drives," *IEEE Transactions on Power Electronics*, vol. 37, no. 12, pp. 15260-15271, Dec. 2022, doi: 10.1109/TPEL.2022.3189876.

[21] J. Chen, Y. Qin, A. M. Bozorgi and M. Farasat, "Low Complexity Dual-Vector Model Predictive Current Control for Surface-Mounted Permanent Magnet Synchronous Motor Drives," *IEEE Journal of Emerging and Selected Topics in Power Electronics*, vol. 8, no. 3, pp. 2655-2663, Sept. 2020, doi: 10.1109/JESTPE.2019.2917865.

Puli Rajanikanth received the B.Tech. degree in Electrical and Electronics Engineering from Jawaharlal Nehru Technological University, Hyderabad, India, in 2013, and the M.Tech. degree in Electrical Engineering from the National Institute of Technology, Warangal, in 2018, where he is currently pursuing the Ph.D. degree with the Department of Electrical Engineering. His research interests include power electronics, control of multi-phase induction motor and permanent magnet synchronous motor (PMSM) drives.

Vinay Kumar Thippiripati received the B.Tech. and M.Tech. degrees in Electrical Engineering from Jawaharlal Nehru Technological University, Hyderabad, India, in 2005 and 2008, respectively. He received the Ph.D. degree in Electrical Engineering from the National Institute of Technology, Warangal, India, in 2015. In 2013, he joined in National Institute of Technology, Warangal, India, as an Associate Professor. His research interests include power electronics and drives, direct torque control, predictive torque control, open-end winding induction motor drives, multilevel inverters, hybrid electric vehicles, and renewable energy interfacing.